New Generation Free-Space Optical Communication Systems With Advanced Optical Beam Stabilizer

Abdelmoula Bekkali, *Senior Member, IEEE*, Hideo Fujita, and Michikazu Hattori

(Top-Scored Paper)

***Abstract*—In this paper, we introduce a novel concept and design of a full-duplex and all-optical FSO transceiver and evaluate its transmission performance in 200 m outdoor environment. Our transceiver enables a reliable fiber-to-fiber FSO link with intelligent lens-based optical-beam-stabilization (OBS) by utilizing miniaturized and cost-effective 3-axis voice-coil motors (VCMs) actuators. The VCM-based moving lens that is widely used in smartphone cameras for auto-focus and optical-image-stabilization is customized and optimized for our designed transceiver to expand the transmitter and receiver field-of-view, control both the transmitted and incident laser beam alignment, suppress the effects of random beam angle-of-arrival fluctuations induced by the atmospheric turbulence and pointing errors and maintain efficient direct coupling to the fiber core at the receiver. Unlike the 2-axis fast-steering-mirrors, the use of 3-axis VCM lenses can not only maintain the beam alignment, but also control the beam collimation and adjust the difference between the lens focal plane and projection plane for a higher fiber coupling efficiency. Using our developed FSO transceivers, we demonstrate an error-free transmission of the standard signals 10 GbE LAN and common public radio interface (LTE-CPRI) over 200 m links. We also performed a continuous 24-h transmission evaluation in a clear weather day, with only occasional burst errors were recorded and a total 24-h BER of 3×10^{-10}. The obtained results demonstrate the potential of our proposed FSO transceiver to ensure high-capacity communication links and facilitate the adoption of the FSO system as a viable candidate to address the main requirements of B5G/6G networks.**

***Index Terms*—Free-space optics (FSO), optical beam stabilizer (OBS), voice-coil motors (VCM), fast steering mirror (FSM), all-optical FSO, pointing acquisition and tracking (PAT).**

I. Introduction

With the ever-increasing of global mobile data traffic, there is a consensus that 5G/6G networks will enable faster data speeds, higher capacity, lower latency, and massive connectivity [1]. These requirements will lead to almost similar performance to the current fiber-to-the-home services, and thus they will pose a huge challenge to the legacy optical access network [2], [3]. Despite the clear advantages of the optical fiber communications for 5G/6G networks, the lack of deployment flexibility, resiliency and cost make their operation challenging, especially in dense urban areas, as well as remote areas lacking fiber infrastructure [4], [5]. Moreover, the Telecom operators need continuously to dig up streets and install new equipment required to connect a large number of their sprawling central offices (COs). To address these issues, free-space optics (FSO) system has been recognized as a promising wireless interconnecting technology for high-capacity, cost, and energy-efficient communication networks ensuring data-rate similar to that provided by optical fiber links, but at a fraction of their deployment cost [5]–[10]. The wireless feature of the FSO link enables an agile and resilient communication system, for both dense urban and rural areas, as well as areas that are likely susceptible to outages from fiber cuts.

The FSO communication bands are license-free and have abundant bandwidth spanning from visible to infrared (IR) bands, where the available spectrum depends mainly on the transmission window of the atmosphere. For instance, for the IR-based FSO system, the available transmission windows are 850, 1310, and 1550 nm bands, which coincide well with the standard optical fiber communication. Despite its potential advantages, the FSO link has certain inherent limitations and challenges that should be addressed carefully for a stable and reliable communication system. These challenges include absorption and scattering loss (e.g. fog, rain,..), and atmospheric turbulence (e.g. beam wander, scintillation) [11], [12]. Furthermore, the FSO link is restricted to stringent line-of-sight (LOS) requirements, which requires advanced pointing, acquisition, and tracking (PAT) techniques [13].

Recently several research efforts have been proposed to design reliable and high-capacity FSO systems, from fixed terrestrial to high-altitude moving platforms (i.e. drones, satellites) [10], [14]–[22]. To increase the system reliability and field-of-regard, the beam tracking is usually split into coarse and fine tracking modules, which corresponds to the alignment process of the incident beam to the antenna telescope lens and the fiber-core or PD apertures, respectively. For rough tracking, the current systems typically implement 2-axis gimbals and/or larger aperture fast steering mirrors (FSMs), while for fine tracking miniaturized FSMs are commonly used [14], [15]. The FSMs can deflect and steer accurately the incident beam onto the receiving aperture and they are developed using three types of actuators: mechanical, piezoelectric (PZT), and micro-electromechanical systems

Manuscript received July 31, 2021; revised November 15, 2021 and January 8, 2022; accepted January 18, 2022. Date of publication January 27, 2022; date of current version March 2, 2022. *(Corresponding author: Abdelmoula Bekkali.)*

The authors are with R&D Center, TOYO Electric Corporation, 486-8585 Kasugai-shi, Aichi, Japan (e-mail: bekkali_a@toyo-elec.co.jp; hideo_fujita@toyo-elec.co.jp; mitikazu_hattori@toyo-elec.co.jp).

Color versions of one or more figures in this article are available at https://doi.org/10.1109/JLT.2022.3146252.

Digital Object Identifier 10.1109/JLT.2022.3146252

(MEMS) [16]. In [17], [18], the authors proposed a typical FSO transceiver with gimbal and beacon signals for rough tracking and large bandwidth FSM for fine tracking. Using a similar design, multiple standard wireless signals [19] and 1.28 Tbps digital signal [10], were successfully transmitted. In these systems, a fiber-optics-based optical circulator was used to enable full-duplex transmission. However, with this circulator, it is not possible to control independently the optical path of the transmitter and receiver. Another typical design for satellite laser communication systems was proposed in [20], [21]. Here, the authors developed an FSO transceiver with FSM for fine tracking, while for rough tracking, they implemented an attitude determination and control systems (ADCS) with the cubesat body pointing. To enable full-duplex transmission, the authors implemented a polarization beam splitter and assigned separated wavelengths for transmission and reception. However, this technique may not be practical for fiber-to-fiber systems, where the optical signal polarization remains a challenging issue. In [22], the authors proposed a high speed retro-reflective FSO system between ground station and unmanned aerial vehicle (UAV). In this system, the gimbal was used for trough tracking, while for fine tracking/pointing, two separated modules were implemented for transmission (i.e. spatial light modulator (SLM)) and reception (i.e FSM). To enable full-duplex transmission, the optical system was arranged in a bi-static configuration. Indeed, this design can improve the isolation between both two optical paths, but it will increase the link loss and the transceiver mass and size.

In this paper, we introduce the design and concept of our newly developed full-duplex all-optical FSO transceiver. Unlike the existing FSO system that is based on 2-axis FSM technology, we propose to utilize a miniaturized cost-effective 3-axis voice-coil motors (VCMs)-based movable lens [23], [24]. Using this technology, we can implement the tracking module with a similar performance to the FSM, but with a simpler optical path design, especially when used for fiber coupling. Indeed, we can not only maintain the beam alignment as for FSM, but also we can control the beam collimation and adjust the difference between the lens focal plane and projection plane for a higher fiber coupling efficiency.

The VCM lens, that is widely used in the current smartphone and digital cameras for auto-focus (AF) and optical image stabilization (OIS) functionalities [25], is customized and optimized for our newly designed transceiver to (i) expand the transmitter and receiver FOV, (ii) control both the transmitted and incident beam alignment, (iii) suppress the effects of random beam angle-of-arrival (AOA) fluctuations induced by the atmospheric turbulence and pointing errors, and (iv) maintain efficient direct coupling to the fiber core at the receiver.

To enable full-duplex transmission, we also developed for the first-time an polarization-independent free space-based optical circulator (FSO-C) which can ensure similar flexibility as the binocular transceiver, so that the transmitted and received beams can be controlled efficiently and independently. Our FSO-C is based on similar design of the fiber-optic optical circulators. Utilizing a single transmitting and receiving lens, the FSO-C will not only enable full-duplex transmission but also eliminate the impact of the optical antenna *roll*, which is critical for binocular FSO transceivers on moving platforms.

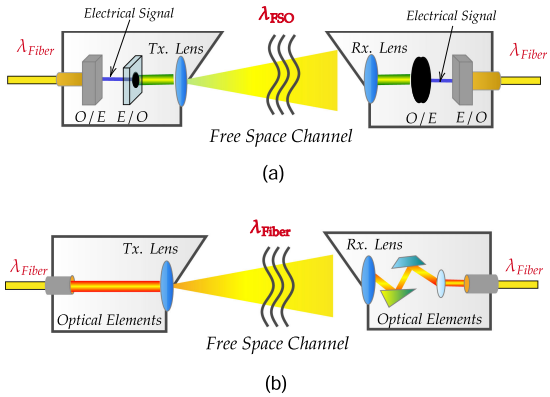

Fig. 1. General architecture of FSO system: (a) Mixed electrical-optical FSO. (b) All-optical FSO system.

In this paper, we introduce the design and concept of our newly developed full-duplex all-optical FSO transceiver and evaluate its performance in a 200 m outdoor environment. Our transceiver enables fiber-to-fiber (F2F) communication system with dynamic optical-beam-stabilization (OBS) by utilizing a cost-effective 3-axis VCMs movable lens [23], [24]. To maintain a dynamic laser beam pointing and tracking control, we developed and implemented an intelligent coordination algorithms between all VCM actuators using the received optical power and quadrant photodetector (QPD) sensor data. These control algorithms allow us to optimize the 3D position for all lenses so that the received optical power coupled to the fiber core can be maximized and stabilized.

Using our developed FSO transceivers, we demonstrate an error-free transmission of the standard signals 10 GbE LAN and 10 channels of common public radio interface (LTE-CPRI) over 200 m free-space links. Two different scenarios were considered: (i) reflected-back using a ϕ50 mm corner-cube and (ii) loop-back by directly coupling the received optical signal to the transmission port after amplification.

The rest of this paper is organized as follows: the architecture of all-optical FSO system and its enabling technologies are introduced in Section II, where the advantages and differences between mixed and all-optical FSO system are explained. Then, we provide a detailed concept and operation of our OBS technology. In Section III, we present our proposed full-duplex all-optical FSO transceiver with an integrated FSO-C and dynamic OBS. The experimental setup and outdoor transmission evaluation are presented and discussed in Section IV. Finally, conclusions are given in Section V.

II. FSO System Architecture and Transceiver Design

In general, the FSO system can be developed using two main architectures: (i) mixed electrical-optical FSO and (ii) all-optical FSO. Fig. 1 illustrates the general overview of mixed and all-optical FSO system.

A. Mixed Electrical-Optical FSO Transceivers

The existing commercial systems are based on mixed electrical-optical FSO transceivers which rely on the implementation of O/E, E/O converters as well as signal processing

blocks at the transceiver terminal. Fig. 1(a) illustrates a general architecture of the mixed electrical-optical FSO system. This system typically operates at wavelengths that lie from visible to near-IR bands and can have wider FOV. Basically, this system implements wide beam divergence at the transmitter and large diameter surface-illuminated photo-diode (PD) at the receiver, which makes the pointing and tracking mechanisms very relaxed. However, the transmission bandwidth and data rate are always limited by the used O/E and E/O characteristics and performance. In order to improve the system capacity, a broadband PD with high receiver sensitivity is required. In fact, there is a trade-off between the surface-illuminated PD active area and its electrical bandwidth [26], [27]. Therefore, to enable a larger bandwidth FSO transceiver, a smaller aperture PD with a focusing lens will be utilized, leading to a smaller FoV and thus an active beam tracking mechanism and/or PD array should be implemented.

B. All-Optical FSO Transceivers

In order to satisfy the main requirements of B5G/6G networks in terms of capacity, scalability, flexibility, and low latency, it is desirable to use only optical elements (e.g. lenses, mirrors,..) for both transmitter and receiver. In this scenario, the O/E and E/O blocs should be omitted at the FSO transceiver leading to a seamless integration of optical fiber and free-space links with direct fiber-coupling, as depicted in Fig. 1(b). Such system also referred to as all-optical FSO, will be compatible with the existing fiber infrastructure, as well as protocol and waveform transparent. Using the 1310/1550 nm window, multi-Gbps wireless transmission can be achieved by leveraging the technology developed for optical fiber communication such as erbium-doped fiber amplifier (EDFA), semiconductor optical amplifier (SOA), large bandwidth PD (e.g. uni-traveling carrier photodiodes (UTC-PD)), and wavelength-division multiplexing (WDM), as well as the new generation of small form-factor pluggable (e.g. SFP+, QSFP28,...) optical modular transceivers that are widely used for both telecom and data communications applications. Moreover, all-optical FSO system will be compatible with the high capacity analog radio-over fiber system which is considered as a potential candidate for B5G/6G networks [28]–[30]. However, they require advanced laser beam pointing and tracking control mechanism.

The beam tracking can be split into coarse and fine tracking, which corresponds to the alignment process of the incident beam to the antenna telescope lens and the fiber-core apertures, respectively. Fine tracking is crucial for all-optical FSO system and is usually performed using fast steering mirrors (FSMs) [10], [19]. Using controlled 2-axis actuators, the FSM can deflect and steer accurately the incident beam onto the receiving aperture. However, the optical path is difficult to design and the system is costly especially when used for fiber coupling.

C. Optical Beam Stabilizer Approach

As an alternative to the FSM technology, we propose a novel approach for pointing and tracking mechanism based on lens-based OBS [23], [24]. The OBS is implemented using a

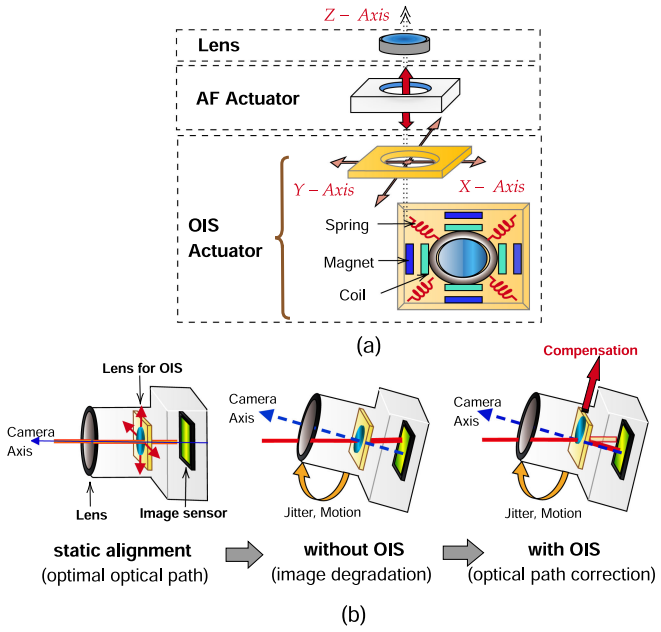

Fig. 2. (a) Overview of VCM lens structure. (b) Basic principle of OIS for cameras.

cost-effective 3-axis VCM actuator, which is widely used in the current smartphones and digital cameras for AF and OIS modules, owing to its low cost, low power consumption, quick response, and small size. Fig. 2(a) shows the basic structure of the VCM actuator. The OIS technique consists of physically moving the camera lens to compensate for image quality degradation and blurring induced by the natural hand jitter and camera motion. As illustrated in Fig. 2(b), by moving the lenses, the OIS can control and adjust the optical path between the target and image sensor, and thus the received image can be kept steady.

The VCM actuator is a direct drive motor that can achieve high precision position servo control. It has many applications in the field of high-frequency reciprocating linear motion. The VCM operates using a simple principle of electromagnetism so that when electricity passes through a coil, it produces a magnetic field that reacts with a permanent magnet to either repel or attract the coil. In general, the VCM actuator consists of two main modules. The first module is fixed and includes two magnets, known as yoke and base, while the second module is moving and has the lens with holder attached using coils [25]. Thus, based on the Lorentz-Force principle, the lens can be moved by a distance that is directly proportional to the current applied to the coil.

In order to implement the OBS feature in the FSO transceiver using VCM actuators, several important characteristics and parameters should be taken into consideration, which include:

1) *Transfer curve:* the relationship between applied current and VCM actuator displacement. The 3-axis VCM displacements and lens movements are detected using a *hall sensor*, which is part of the VCM actuator.
2) *Stroke:* the largest displacement that the VCM actuator can make, which usually corresponds to the maximum applied current. Depending on the transceiver optical design, a

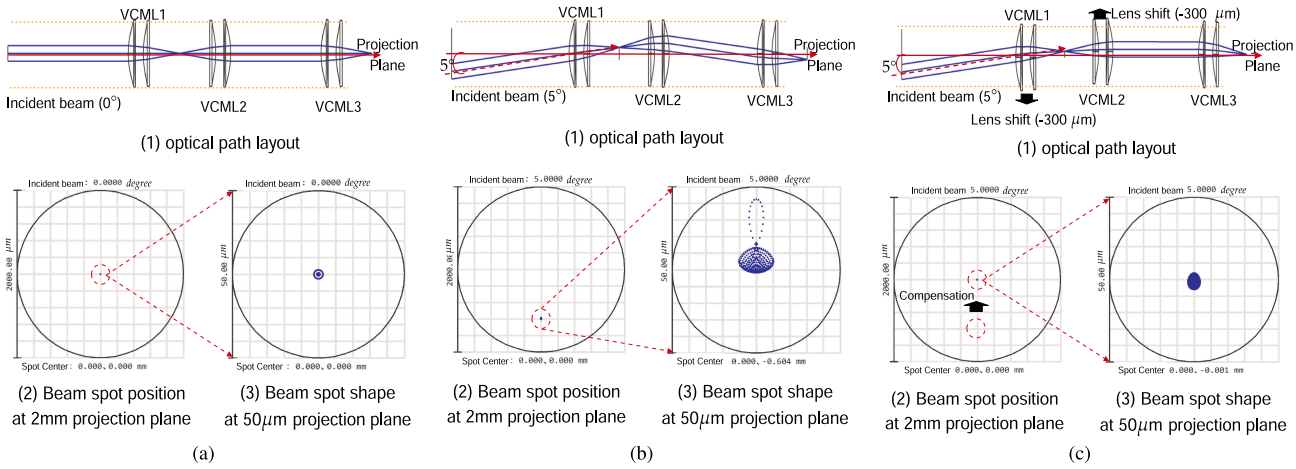

Fig. 3. Concept of VCM lens operation using Zemax simulation. (a) Static alignment with optimal optical path. (b) Beam spot deviation without VCM lens compensation. (c) Beam spot deviation with VCM lens compensation.

larger stroke can lead to higher FoV and can give more flexibility to the lens movement.

3) *Linearity:* the VCM stroke exhibits a linear relationship with the applied current and thus the movement of the lens to the desired position can be easily controlled. Also, simpler and faster control algorithms can be implemented.
4) *Hysteresis:* the position deviation when the VCM moves forward and backward at the same current value. Typically, the VCM has low hysteresis. In fact, for the case of all-optical FSO system, motors with larger hysteresis may lead to the received optical power fluctuation during feedback control.
5) *Slope:* which describes both the direction and steepness of the VCM transfer curve. The slope can define the lens displacement control resolution and direction. It is important for stability and control accuracy.
6) *Speed and bandwidth:* which describes how fast the VCM responds. The VCM speed and bandwidth are very crucial to mitigate the high-frequency beam misalignment induced by scintillation and beam wander.
7) *Gravity:* when the lens moves upward and downward, the gravity of the lens may be added to the electromagnetic force. Hence, a compensation force balance should be considered.

The miniaturized VCM-based lens can provide high beam steering performance and quick response at a lower cost. To better clarify the VCM lens operation for compensating the beam deviation, we performed a ray-tracing simulation of the optical path using the Zemax OpticsStudio simulator [33]. As illustrated in Fig. 3, The optical system consists of two lenses (i.e. VCML1 and VCML2) that will be used for steering and another lens (i.e. VCML3) for focusing on the projection plane. The focal length of each lens is 5 mm. For reference, we plotted in Fig. 3(a), the laser path simulation for straight and static beam alignment. As shown in Fig. 3(b), when the incident beam is deviated by 5 degrees, the laser beam spot position is largely shifted from the center (0 μm, 0 μm) to about (0 μm, -600 μm). Furthermore, due to the chromatic aberrations, laser spot deformation can also be observed. In Fig. 3(c), it is clear that by simply shifting the VCM1&2 lenses to the appropriate position, the laser spot deviation can be fully compensated. For instance, in order to compensate the 5 degrees beam deviation, the VCML1 and VCML2 should be shifted in the y-direction by -300 μm and +300 μm respectively. Unlike the 2-axis FSMs-based system, the use of 3-axis VCM lenses can not only maintain the beam alignment but also control the beam collimation and adjust the difference between the lens focal plane and projection plane for a higher fiber coupling efficiency.

III. All-Optical FSO Transceiver With Dynamic Optical Beam Stabilization

In this section, we introduce the concept and design of our novel all-optical and full-duplex FSO transceiver based on FSO-C and OBS technologies. First, we show the configuration of internal antenna optical devices and optical layout design, then we introduce the implemented control block diagram and the operation of each block. In this FSO terminal, the FSO-C and OBS systems were designed, optimized and developed to get higher performance transmission.

A. FSO Transceiver Design

The optical path and system layout of our proposed FSO transceiver is depicted in Fig. 4(a). Five VCM actuators were implemented to control the 3-axis position of the lenses that are placed on the receiving and transmitting optical path, and thus the received light deflection angle and fiber coupling can be controlled efficiently. As shown in Fig. 4(b), the size of our miniaturized VCM actuator and lens are 12 mm $\times$ 12 mm $\times$ 5 mm and ϕ8 mm, respectively.

To enable fiber-to-fiber and full-duplex transmission, we developed for the first time a 3-ports polarization independent FSO-C, that has similar characteristics of the fiber-based optical circulator. It consists of four main components, i.e., 45° Faraday rotator (FR), half-wave plate (HWP), a polarizing beam splitter

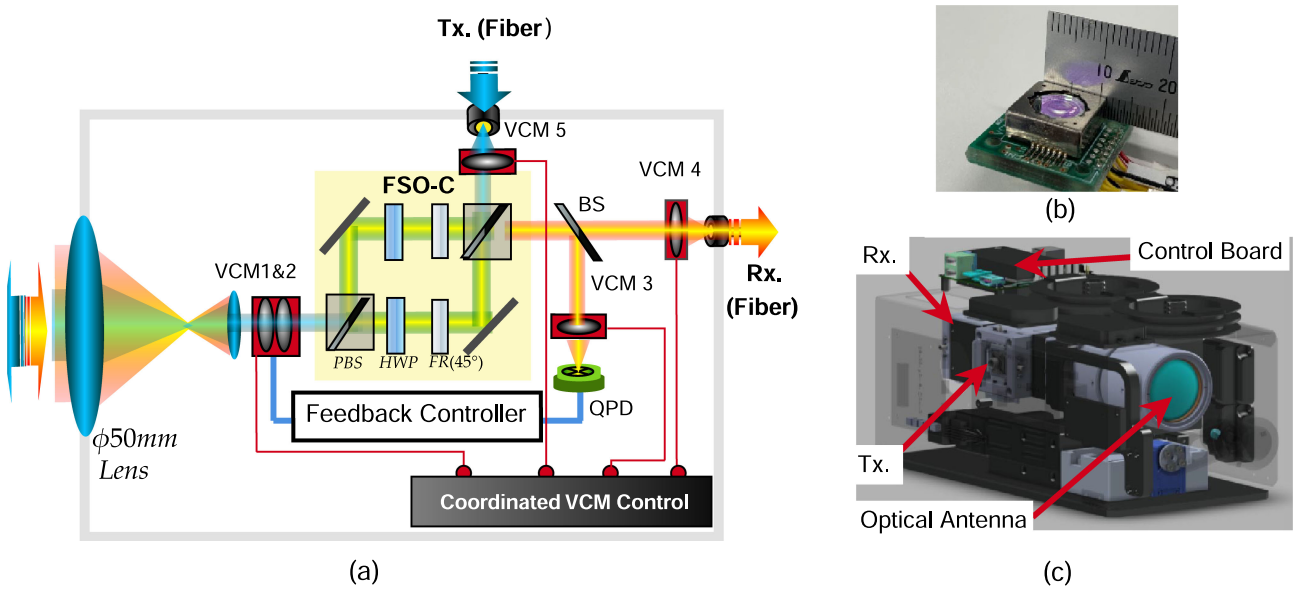

Fig. 4. Our proposed all-optical FSO transceiver design. (a) Optical path and system layout. (b) Photograph of our used VCM lens. (c) Transceiver overview.

(PBS), and a prism mirror. In this circulator, the isolation between the three ports is more than 25 dB and the insertion loss is less than 0.5 dB. Unlike the fiber-based optical calculator that can be placed at the receiving port of the FSO transceiver, the FSO-C can enable efficient and independent control of the transmitted and received beams similar to the binocular FSO transceiver, which leads to a simple and flexible optical path design. Indeed, utilizing a single transmitting and receiving lens, the FSO-C will not only enable full-duplex transmission but also eliminate the impact of the optical antenna *roll*, in particular for narrow beam FSO links and moving platforms.

By adjusting the 3D position of the VCM5 lens, the incoming laser beam transmitted from the SMF is aligned and expanded to the $\phi 2$ mm beam. The collimated beam passes through the FSO-C, and then undergoes a 1:7.5 beam expansion process to $\phi 15$ mm, before being transmitted to the air. At the Rx. side, the beam is received using a $\phi 50$ mm lens, aligned using VCM1&2, passed through the FSO-C, and then seamlessly coupled to the fiber core using both the fine tracking module based on VCM1&2 and the fiber coupling module that is based on VCM4. To operate the fine tracking module, we used a 10:90 beam splitter and a QPD as a tracking sensor. In fact, the QPD sensor outperforms the image sensors in terms of beam position accuracy and response time [31]. In order to focus the beam to the QPD sensor, we placed another VCM actuator (i.e VCM3), where the lens position (x,y) was initially adjusted so that the laser beam spot is centered at the QPD aperture, while its z-value is used to control the beam spot size. The tilted angle of the received wavefront was estimated and used by the proportional-integral-derivative (PID) controller for ordering the VCM1&2 to minimize the deflection angle.

In this terminal, we implemented a commercial VCM actuator that was specifically designed for smart-phone cameras, where its available control bandwidth can reach up to 100 Hz. In our system, the control bandwidth was limited to up 100 Hz, due to (i) the used off-the-shelves VCM technology bandwidth (that is developed for smartphone camera), (ii) the closed-loop servo bandwidth and (iii) the movable lens weight. The parameters of the PID controller was adjusted carefully for both x and y directions to increase the bandwidth by as high as possible.

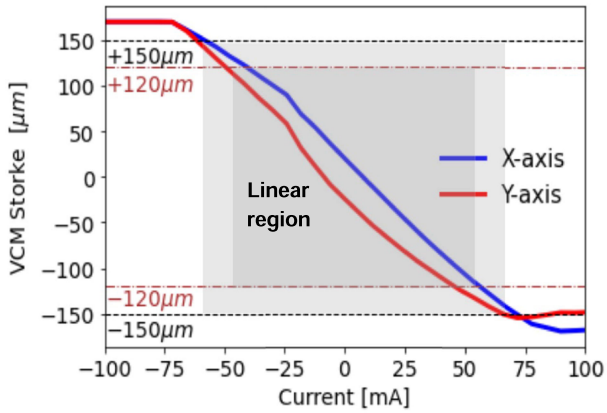

Fig. 5. VCM actuator stroke vs. applied current.

Fig. 5 illustrates the x- and y-axis response of our VCM stroke (μm) with the applied current (mA). From the figure, by changing the current between -50 mA and $+50$ mA, the VCM will move linearly from $-120\,\mu$m to $+120\,\mu$m, with a full stroke of $240\,\mu$m and can reach even $300\,\mu$m. Hence, by maintaining the VCM displacement at the linear region, we can easily control the movement of the lenses to the desired position. In our design, the hysteresis tolerance and gravity of the lens system have been taken into account for higher performance of upward and downward displacement.

To allow maximum coupling efficiency, the VCM4 z-value was controlled so that the focused spot size becomes comparable to the fiber core size. According to Gaussian optics, in order to

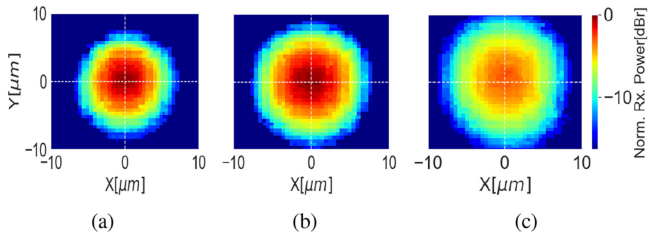

Fig. 6. Received optical power profile for different z value of VCM4. (a) $z = 0$. (b) $z = -90\,\mu$m. (c) $z = -175\,\mu$m.

couple a collimated laser beam with wavelength λ and diameter D_B into a fiber of mode field diameter d_F, the coupling lens focal length should be $f = \frac{\pi D_B d_F}{4\lambda}$. Fig. 6 plots the received optical power profile for VCM 4 that is used for fiber coupling. The power data were measured using 10μm SMF core and by moving the VCM4 lens positions x and y in a spiral way and for different z positions (i.e. 0μm, -90μm and -175μm). Thanks to the VCM linearity, we can easily control the fiber coupling efficiency for better system performance. Indeed, for the incident collimated beam, the power profile at the fiber core also shows Gaussian behavior. Hence, by modifying the z value, the power profile size and peak power can be controlled efficiently.

B. OBS Design and Implementation

In our FSO transceiver, the OBS system incorporates different modules and components for sensing, compensation, and control to accurately correct the incoming beam on-axis deviation, as well as, the optical antenna movement, such as the *pan-tilt* deviation. Using the received optical power and the QPD sensor data, we implemented the OBS system based on an intelligent coordination algorithm between all five VCM and gimbal actuators, so that a dynamic pointing and tracking control can be maintained. These algorithms allow us to optimize the 3D position for all lenses, where the received optical power coupled to fiber core can be maximized and stabilized. By placing the fine tracking VCM (i.e. VCM1&2) between the FSO-C and transceiver telescope enables simultaneous alignment control of both received beam with the fiber core, and the transmitted beam with opposite antenna aperture. Therefore, the two FSO antennas can cooperate and maintain on-axis transmitting and receiving beams, without the need for external communication tools.

Fig. 7 illustrates the block diagram of the five main control processes that are used for (i) beaconless initial alignment (ii) tracking/pointing, and (iii) fiber coupling. In the following, we describe in detail each module and how the control processes are implemented:

1) Beaconless Initial Alignment: At the first step, we use a guide-scope to reduce the acquisition uncertainty area by adjusting the antennas heading direction. Then, we place a ϕ15 mm corner-cube at the center of the opposite antenna aperture, so that the reflected beam and the expected actual received beam from the opposite antenna can be on-axis. Next step, we start the beaconless initial alignment by scanning the two-axis gimbal in a spiral way within the acquisition uncertainty area, until the reflected beam from the corner-cube is detected by the ϕ3 mm QPD sensor (Fig. 7: Gimbal Process. We then repeat the scanning process with a smaller resolution step until the received optical power is maximized. Since our used 2-axis gimbal scanning resolution is low (i.e. 17 μrad), we improve the received optical power by scanning the laser beam in a spiral way using the VCM5 actuator, which has a resolution step of 2.5 μrad (Fig. 7: VCM5 Process). In the VCM5 process, we can also select the appropriate beam divergence for initial alignment by controlling the z-position of the VCM5 lens. For instance, by increasing the beam divergence, the scan resolution step can be increased and thus the acquisition time can be reduced. Moreover, by adjusting the (x,y)-position of the VCM5 lens, we can control the "*point ahead angle*" (PAA) [32], which is a critical parameter, especially when the relative angular velocity of the two FSO transceivers increases.

For the second transceiver, we use similar process done for the first antenna using another corner-cube placed at the center of the first antenna aperture.

Next, we remove the corner-cube and we evaluate the received optical power, using the actual received beam from both transceivers. Here, we may need to adjust slightly the lenses position of the VCM3 (Fig. 7: VCM3 Process) and the VCM4 (Fig. 7: VCM4 Process), so that the beam spot and position at the QPD sensor are optimized and the received optical power at the fiber core is maximized.

2) Tracking Module: In order to design all-optical FSO system with direct coupling to the fiber core, two main tracking modules should be implemented:

a) *Coarse tracking module:* which enables the alignment of the incident laser beam axis with the normal axis of the receiving antenna (i.e. telescope) aperture. The coarse tracking system is also used for initial alignment and typically implemented using two-axis gimbal, acquisition sensor (e.g. CCD camera) and reference beacon with large beam divergence. In our transceiver, we adopt beaconless coarse tracking system, where the ϕ3 mm QPD sensor can be used.

b) *Fine tracking module:* which is most critical for all-optical FSO transceivers. It enables the alignment of incident laser beam axis with the normal axis of the fiber core aperture. The beam tracking system typically consists of (i) *a tracking sensor* such as QPD and (ii) *a beam-steering device*, such as mirror-based FSM. In our transceiver, we adopt VCM lens-based OBS.

Combining the two tracking modules, a more effective tracking mechanism can be realized. Fig. 8 shows the schematic diagram of our tracking controller. The tilted angle of the received wavefront as a result of AOA fluctuations is detected by the QPD and the corresponding beam relative deviation from the QPD center is calculated. This position will be used by the PID controller to calculate the required 2D shift control for the VCM1&2 lenses so that the deflection angle is minimized.

Since the transmitted beam divergence is narrow (i.e. 120 μrad) and the antenna aperture size is small (i.e. ϕ50 mm), the FSO link is susceptible to antennas misalignment. In order to maintain the laser beam inside the QPD sensor control zone, we

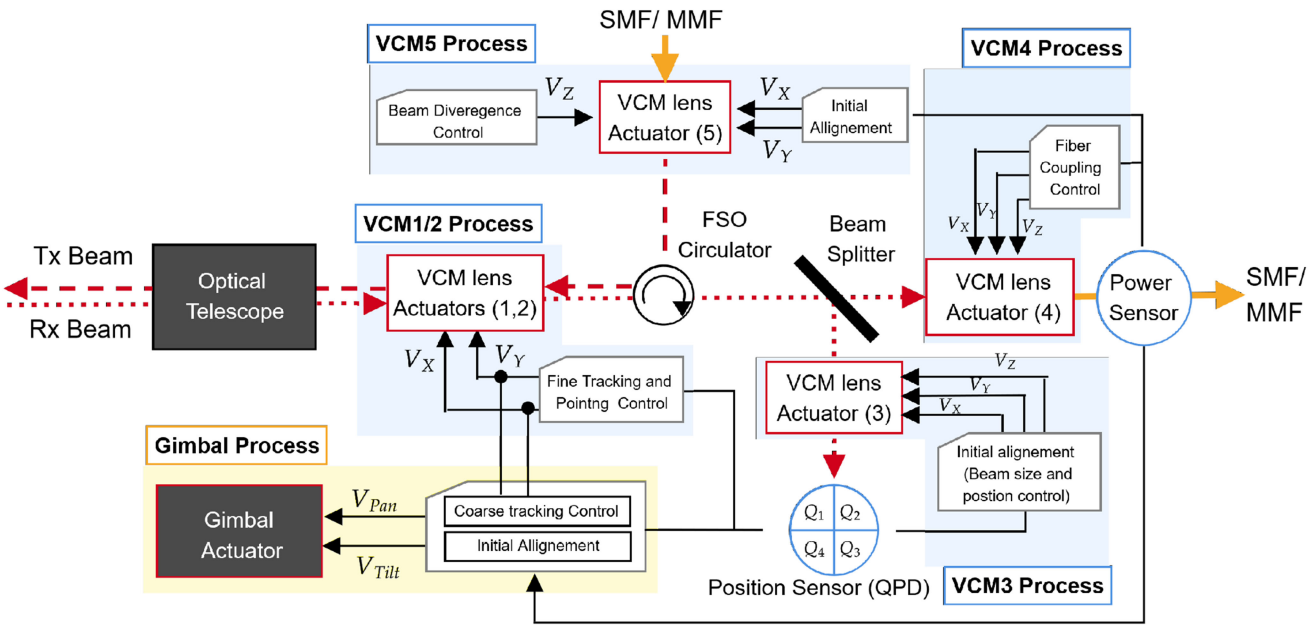

Fig. 7. Block diagram of the five main control processes that are used for beaconless initial alignment, tracking/pointing and fiber coupling. V_X and V_Y indicate actuator's X and Y voltages.

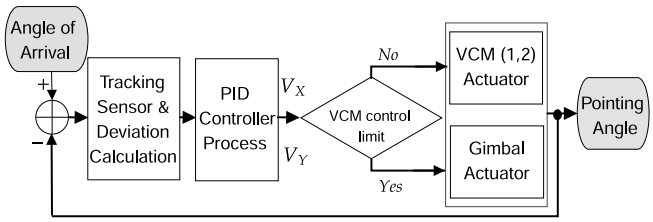

Fig. 8. Control loop diagram for FSO tracking system.

set dynamic upper- and lower-bound values for the VCM shift control. Hence, when the VCM actuator reaches the control zone boundaries, we order the gimbal actuator to move and bring back the received laser beam to the control zone.

IV. Experimental Transmission and Evaluation

In order to evaluate the transmission performance of our full-duplex and all-optical FSO system, two developed transceivers, TRx1 and TRx2, were placed in an outdoor environment within the TOYO Electric factory premise and separated by a distance of 100 m. A schematic diagram representing the experimental setup of the FSO system is shown in Fig. 9. For the evaluation purpose, we assigned different beam divergence to each transceiver, which is 120 μrad and 870 μrad for TRx1 and TRx2, respectively.

To investigate the efficiency of our pointing and tracking mechanism using the OBS with coordinated VCM control, we modified the vertical position of TRx1 upward and downward within a range of 30 cm, which is limited by the maximum adjustable height of the used tripods. The normalized received optical power for different values of the up and down deviation from -10 cm to 20 cm is shown in Fig. 10. Here the TRx.2 is the transmitter, while TRx.1 is the receiver. When the OBS control is OFF, the optical power drops by 30 dBr for a deviation position less than ± 1 cm. By applying the OBS control at the TRx1, the controlled deviation could exceed ± 4 cm and ± 7 cm, with -3 dBr and -9 dBr degradation respectively. On the other hand, by activating simultaneously the OBS control of both transceivers and assuming that the received beam is Gaussian, the controlled deviation could reach up to ± 13 cm and ± 20 cm with 3 dBr and 9 dBr degradation, respectively.

Fig. 11 illustrates the OBS performance with pointing error. In this evaluation, we checked the received power at TRx1 while modifying the VCM 5 (x,y) values of the TRx2 in a spiral way. From the figure, It is clear that $\pm 0.05\,\mathrm{deg}$ can be controlled efficiently at a distance of 100 m. Our coordinated OBS control for the pointing and tracking system ensures a significant improvement of the receiver FOV with less complexity and minimum electronic overhead. Moreover, our proposed system shows potential for application in moving platforms and building sway.

To further evaluate the performance of our OBS system, the received power fluctuation control on a clear and windy day was measured and plotted in Fig. 12. The power data was collected every 1 ms and the wind speed was about 14 m/s. Since the TRx was placed on the tripod, the strong wind led to antennas misalignment power fading (i.e. pointing error). From the figure, when the OBS was OFF, the impact of the wind was large. However, by activating the OBS control, the deep power fading fluctuation was successfully eliminated.

We used a bit-error-rate tester (BERT) (Anritsu MP2100 A) for generating two standard signals: 10 channels of LTE CPRI with a total bit-rate of 6.144 Gbit/s and 10 GbE LAN. The generated signal with a PRBS length of $2^{23} - 1$, was converted to

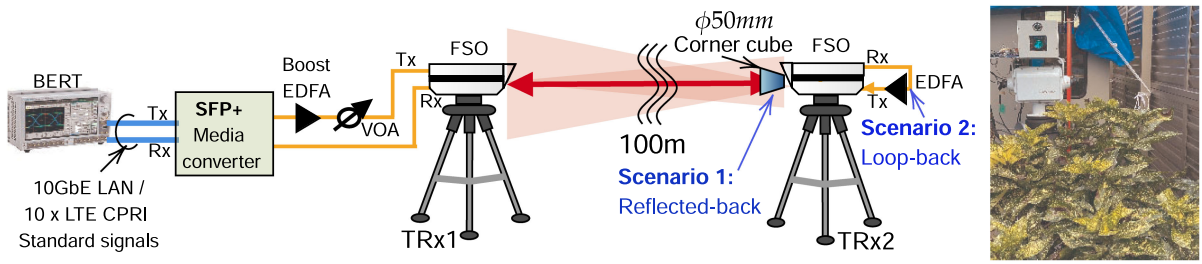

Fig. 9. Experimental setup for our FSO system evaluation.

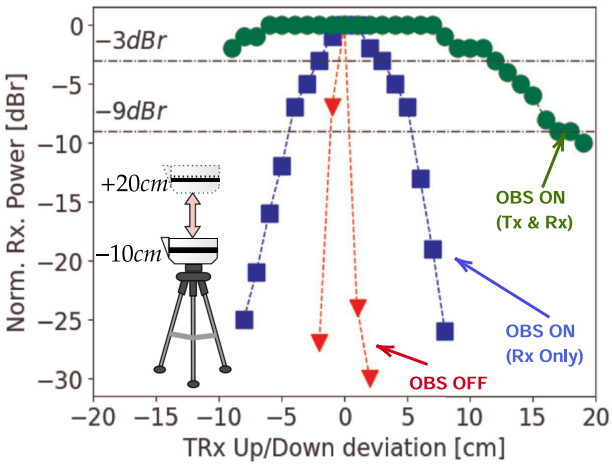

Fig. 10. OBS performance with terminal up and down deviation.

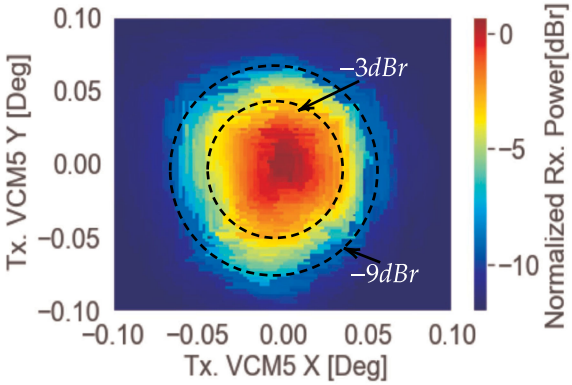

Fig. 11. Controlled received beam with pointing error.

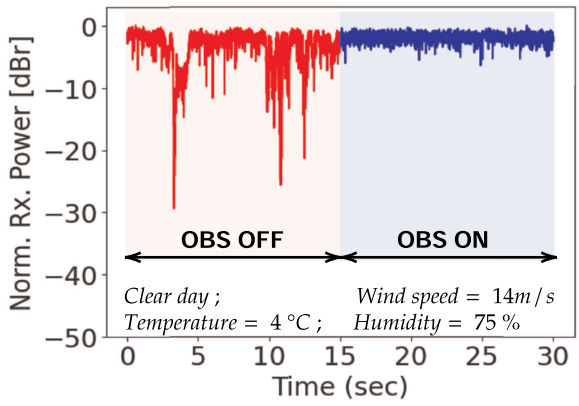

Fig. 12. OBS performance under a clear and windy weather.

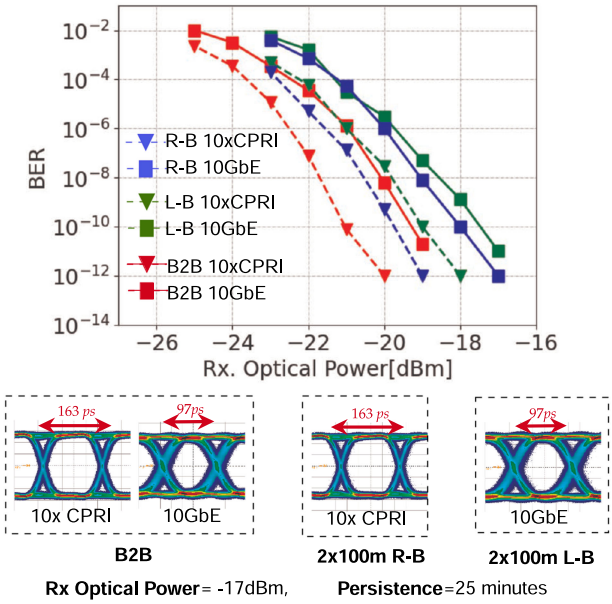

Fig. 13. BER performance for 10 GbE LAN and 10xCPRI signals for B2B, reflected-back (R-B), and loop-back (L-B) scenarios.

the optical signal using an SFP+ media converter, amplified by a boost EDFA, and then directly plugged into the fiber connector of the TRx1. Here, the transmitted optical power was +10 dBm. At the TRx2, two scenarios were considered reflected-back (R-B) using a ϕ50 mm corner-cube and loop-back (L-B) by directly coupling the received optical signal to the transmission port after amplification using another EDFA. The recovered optical signal was then transmitted back to the TRx1, seamlessly coupled to the SMF, and then received by the BERT for evaluation. Fig. 13 depicts the BER curves generated for back-to-back (B2B) and after transmission over 2×100 m reflected- and loop-back links. From the figure, an error-free transmission with a clear open eye diagram can be obtained for both 10 x LTE CPRI and 10 GbE signals, using both scenarios. From the figure and compared to the B2B case, there is less than 1 dB and 1.5 dB power penalty when BER$= 10^{-10}$, for reflected-back and loop-back scenarios, respectively. The insets depict the eye diagram for both received signals with 25 min persistence and optical power of −17 dBm.

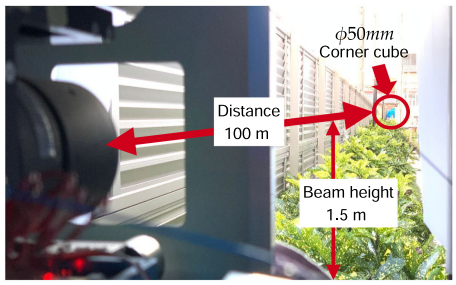

(a)

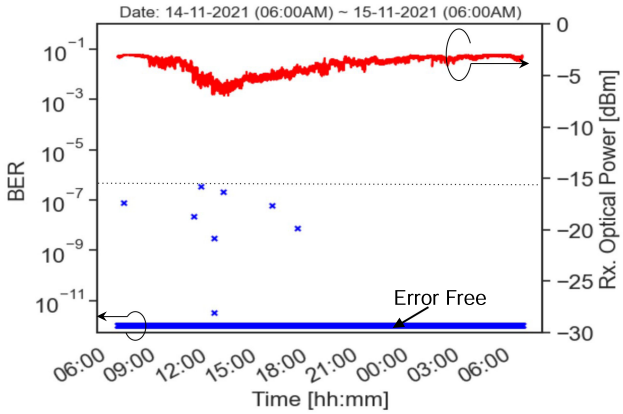

(b)

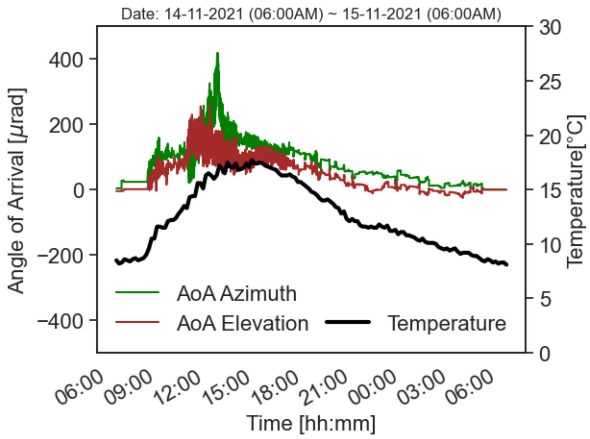

(c)

Fig. 14. 24 h evaluation of the FSO system performance over 200 m reflected-back scenario. (a) Experiment environment and transceiver view. (b) BER values together with the corresponding Rx. optical power. (c) Variation of the temperature and the measured AoA azimuth/elevation angles.

It is clear that no additional degradation and distortion can be observed after transmission using our FSO transceivers.

We also evaluated the BER performance of our FSO system over a continuous 24 h period. We performed real-time transmission of 10 GbE standard signal over a reflected-back 200-m link, where the beam divergence was set to 120 μrad and transmission power is $+10$ dBm. In this experiment, the weather condition was clear, with the recorded temperature that lies from $+8\,^{\circ}$C to $+18\,^{\circ}$C and the relative humidity was about 90% in early morning/dawn and 50% around noon. Since, our FSO transceivers were placed 1.5 m above the soil and 0.5 m above the plants as shown Fig. 14(a), the atmospheric turbulence condition can be characterized as weak to moderate. The BER results and the received optical power characteristics are shown in Fig. 14(b). The measured BER was collected in a period of 30 seconds, while the received optical power was collected every 500 milli-seconds and averaged over a period of 30 seconds. We also plotted in Fig. 14(c), the weather temperature and the measured AoA azimuth and elevation angles, which are calculated from the VCM1 (VCM2) lens X and Y shift (i.e. control) and collected every 1.5 seconds.

From Fig. 14(b), continuous error-free transmission is observed with rare occasional burst errors around noon and the evening. The burst errors that occurred around noon were attributed to the changes in the ambient temperature. From the figure, the few burst errors BER values were less than 4×10^{-7}, the total measured 24-h BER was about 3×10^{-10} and the mean recorded received optical power was about -3 dBm, confirming the stable performance of the FSO transceiver. As can be seen in Fig. 14(c) and during the same time period, the AoA fluctuation is also high, which leads to faster OBS control. Since our used VCM control bandwidth is up to 100 Hz, the fine pointing/tracking mechanism can not suppress all the rapid beam AoA fluctuations due to the insufficient tracking dynamic range. Similar to the VCM-based FSM systems [34], [35] and using customized VCM actuator with closed-loop servo bandwidth up to 1 kHz, the performance of the OBS can be significantly improved for the case of strong turbulence. In fact, the VCM actuator can be developed to steer our designed movable lens, taking into account the lens weight and the required full-stroke for tracking. Moreover, the closed-loop servo bandwidth combined with optimized PID servo controller should be tuned to up 1 kHz. Nevertheless, the OBS technology can compensate the antenna misalignment throughout the day, which is strongly correlated with the temperature. For instance, in this experiment environment, about 400 μrad AoA azimuth and elevation could be controlled.

V. Conclusion

We introduced the concept, design and evaluation of our newly developed FSO transceiver, based on a novel lens-based OBS technology for dynamic laser beam pointing and tracking. Owing to the transceiver optical design and the intelligent coordination between all the VCM actuators, a wider transceiver FOV was achieved, as well as an error-free transmission of the standards 10 GbE LAN and 10 LTE-CPRI channels (at 6-Gbit/s) over a reflected- and loop-back 2×100 m FSO link. We also performed a continuous 24 h transmission of the 10 GbE LAN signal over the reflected-back link in a clear weather day. Only occasional burst errors were recorded with a total BER of 3×10^{-10}. By using wider bandwidth VCM actuator and further improving the OBS software and hardware, the overall FSO system reliability can be significantly increased in the case of strong turbulence.

The obtained evaluation results demonstrate the potential of our proposed all-optical FSO transceiver to ensure reliable high-capacity communication links and thus facilitate the adoption of the FSO system as a viable candidate to address the main requirements of B5G/6G networks.

REFERENCES

[1] White Paper NTT Docomo, Inc, "5G Evolution and 6G," Feb. 2021.

[2] K. Nishimura *et al.*, "Optical access technology for B5G MFH/MBH," in *Proc. Opt. Fiber Commun. Conf.*, 2019, Paper W3J.1.

[3] M. Suzuki *et al.*, "Optical and wireless integrated technologies for future mobile networks," in *Proc. 19th Int. Conf. Transp. Opt. Netw.*, Jul. 2017, Paper We.A2.2.

[4] A. Bekkali, T. Kobayashi, K. Nishimura, N. Shibagaki, K. Kashima, and Y. Sato, "Millimeter-wave-based fiber-wireless bridge system for 8K UHD video streaming and gigabit ethernet data connectivity," *J. Lightw. Technol.*, vol. 36, no. 18, pp. 3988–3998, Sep. 2018.

[5] A. Bekkali, H. Fujita, and M. Hattori, "Free-space optical communication systems for B5G/6G networks," in *Proc. 26th Optoelectron. Commun. Conf.*, 2021, Paper W1A.1.

[6] Y. Hong *et al.*, "Beyond terabit/s WDM optical wireless transmission using wavelength-transparent beam tracking and steering," in *Proc. Opt. Fiber Commun. Conf. Exhibit.*, 2020, Paper W1G.4.

[7] C. B. Naila, K. Wakamori, M. Matsumoto, A. Bekkali, and K. Tsukamoto, "Transmission analysis of digital TV signals over a radio-on-FSO channel," *IEEE Commun. Mag.*, vol. 50, no. 8, pp. 137–144, Aug. 2012.

[8] M. A. Esmail, A. Ragheb, H. Fathallah, and M. Alouini, "Investigation and demonstration of high speed full-optical hybrid FSO/fiber communication system under light sand storm condition," *IEEE Photon. J.*, vol. 9, no. 1, Feb. 2017, Art. no. 7900612.

[9] K. Matsuda *et al.*, "Field demonstration of real-time 14 Tb/s 220 m FSO transmission with class 1 eye-safe 9-aperture transmitter," in *Proc. Opt. Fiber Commun. Conf.*, 2021, Paper F3C.2 PDP.

[10] E. Ciaramella *et al.*, "1.28 Terabit/s (32 × 40 Gbit/s) WDM transmission over a double-pass free space optical link," in *Proc. IEEE Opt. Fiber Commun. Conf.*, 2009. pp. 1–3.

[11] L. C. Andrews and R. L. Philips, *Laser Beam Propag. Through Random Media*. Bellingham, WA, USA: SPIE, 2005.

[12] C. B. Naila, A. Bekkali, K. Wakamori, and M. Matsumoto, "Transmission analysis of CDMA-based wireless services over turbulent radio-on-FSO links using aperture averaging," in *Proc. IEEE Int. Conf. Commun.*, 2011 pp. 1–6.

[13] Y. Kaymak, R. Rojas-Cessa, J. Feng, N. Ansari, M. Zhou, and T. Zhang, "A survey on acquisition, tracking, and pointing mechanisms for mobile free-space optical communications," *IEEE Commun. Surveys Tuts.*, vol. 20, no. 2, pp. 1104–1123, Apr.–Jun. 2018.

[14] A. G. Talmor, H. Harding, and C. C. Chen, "Two-axis gimbal for air-to-air and air-to-ground laser communications," in *Proc. SPIE*, 2016, vol. 9739, pp 129–135.

[15] T. Yamashita, M. Morita, M. Shimizu, D. Eto, K. Shiratama, and S. Murata, "The new tracking control system for free-space optical communications," in *Proc. IEEE Int. Conf. Space Opt. Syst. Appl.*, 2011, pp. 122–131.

[16] R. Kingsbury, T. Nguyen, K. Riesing, and K. Cahoy, "Fast-steering solutions for cubesat-scale optical communication," in *Proc. Int. Conf. Space Opt.*, 2014, pp. 124–130.

[17] Y. Arimoto, "Compact free-space optical terminal for multi-gigabit signal transmission with a single mode fiber," *Proc. SPIE - Int. Soc. Opt. Eng.*, vol. 7199, no. 7, 2009.

[18] K. Kazaura *et al.*, "Performance evaluation of next generation free-space optical communication system," *IEICE Trans. Electron.*, vol. E90-C, no. 2, pp. 381–388, 2007.

[19] A. Bekkali *et al.*, "Performance evaluation of an advanced DWDM RoFSO system for transmitting multiple RF signals," *IEICE Trans. Fundam. Electron. Commun. Comput. Sci.*, vol. 92-A, no. 11, pp. 2697–2705, 2009.

[20] M. Guelman, A. Kogan, A. Livne, M. Orenstein, and H. Michalik, "Acquisition and pointing control for inter-satellite laser communications," *IEEE Trans. Aerosp. Electron. Syst.*, vol. 40, no. 4, pp. 1239–1248, Oct. 2004.

[21] A. C. Casado *et al.*, "Intersatellite-link demonstration mission between CubeSOTA (LEO CubeSat) and ETS9-HICALI (GEO satellite)," in *Proc. IEEE Int. Conf. Space Opt. Syst. Appl.*, 2019, pp. 1–5.

[22] C. Quintana *et al.*, "A high speed retro-reflective free space optics links with UAV," *J. Lightw. Technol.*, vol. 39, no. 18, pp. 5699–5705, Sep. 2021.

[23] A. Bekkali, H. Fujita, and M. Hattori, "Full-duplex FSO communication system utilizing optical image stabilizer and free-space optical circulator," in *Proc. Eur. Conf. Opt. Commun.*, 2020, Paper We2G-5.

[24] A. Bekkali, H. Fujita, and M. Hattori, "Fiber-to-fiber FSO system with advanced VCM controlled laser beam pointing and tracking," in *Proc. Opt. Fiber Commun. Conf. Exhibit.*, 2021, Paper W7E.6.

[25] Y.-H. Chang *et al.*, "Design of miniaturized optical image stabilization and autofocusing camera module for cellphones," *Sensors Mater.*, vol. 29, no. 7, pp. 989–995, 2017.

[26] T. Koonen, K. Mekonnen, F. Huijskens, Z. Cao, and E. Tangdiongga, "Novel broadband OWC receiver with large aperture and wide field-of-view," in *Proc. Eur. Conf. Opt. Commun.*, 2020, Paper Tu2G-6.

[27] T. Umezawa *et al.*, "25-Gbaud 4-WDM free-space optical communication using high-speed 2-D photodetector array," *J. Lightw. Technol.*, vol. 37, no. 2, pp. 612–618, Jan. 2019.

[28] A. Bekkali, S. Ishimura, K. Tanaka, K. Nishimura, and M. Suzuki, "Multi-IF-over-fiber system with adaptive frequency transmit diversity for high capacity mobile fronthaul," *J. Lightw. Technol.*, vol. 37, no. 19, pp. 4957–4966, Oct. 2019.

[29] K. Tanaka, A. Bekkali, H.-Y. Kao, S. Ishimura, K. Nishimura, and M. Suzuki, "First experimental demonstration of 5G mobile fronthaul consisting of cascaded IF-over-fiber links, frequency converters and a channel selector," in *Proc. Eur. Conf. Opt. Commun.*, 2018.

[30] S. Ishimura, A. Bekkali, K. Tanaka, K. Nishimura, and M. Suzuki, "1.032- tb/s CPRI-equivalent rate IF-over-fiber transmission using a parallel IM/PM transmitter for high-capacity mobile fronthaul links," *J. Lightw. Technol.*, vol. 36, no. 8, pp. 1478–1484, Apr. 2018.

[31] I. A. Ivan, M. Ardeleanu, and G. J. Laurent, "High dynamics and precision optical measurement using a position sensitive detector (PSD) in reflection-mode: Application to 2D object tracking over a smart surface," *Sensors*, vol. 12, no. 12, pp. 16771–16784, 2012.

[32] H. Kaushal and G. Kaddoum, "Optical communication in space: Challenges and mitigation techniques," *IEEE Commun. Surveys Tuts.*, vol. 19, no. 1, pp. 57–96, Jan.–Mar. 2017.

[33] Accessed: Jan. 8, 2022. [Online]. Available: http://www.zemax.com/products/opticstudio

[34] T. Shinshi, D. Shimizu, K. Kodeki, and K. Fukushima, "A fast steering mirror using a compact magnetic suspension and voice coil motors for observation satellites," *Electronics*, vol. 9, no. 12, 2020, Art. no. 1997.

[35] T. Yamashita, M. Morita, M. Shimizu, D. Eto, K. Shiratama, and S. Murata, "The new tracking control system for free-space optical communications," in *Proc. Int. Conf. Space Opt. Syst. Appl.*, 2011, pp. 122–131.

Abdelmoula Bekkali (Senior Member, IEEE) received the M.Sc. and Ph.D. degrees from Waseda University, Tokyo, Japan, in 2007 and 2010, respectively. He is currently a R&D Manager with TOYO Electric Corporation, Japan, where he is leading the development of next generation FSO systems for fixed and mobile platforms. Previously, he was a Senior Researcher with KDDI Research Inc. (2014–2019), an Adjunct Lecturer with Waseda University (2012–2019), a Research Scientist with Qatar Mobility Innovation Center (QMIC), Qatar (2011–2014), and a Researcher with NTT Labs, Tokyo, Japan (2010–2011). He holds ten granted Japanese patents in the field of optical and wireless communications. His current research interests include optical wireless communication, free-space optics systems, fiber-wireless systems, millimeter-wave communications, and RFID systems. He was the recipient of the 2016 KDDI Excellent Research Award, 2009 Waseda University Ono Azusa memorial Gold medal, 26th Telecom System Technology Award from the Telecommunication Advancement Foundation (TAF) of Japan, and Best Paper Awards of IEICE Transactions (2009 and 2015), IIEEJ Journal (2012), and IEEE WCNC Conference (2014). He was the ONS Symposium Co-Chair of IEEE Globecom 2020.

Hideo Fujita graduated from the Faculty of Engineering, Gifu National College of Technology, Motosu, Japan, in 1976. Since then, he has been with TOYO Electric Corporation, Japan. He is also leading several R&D projects and commercial products related to Gigabit free-space optics and wireless sensor devices.

Michikazu Hattori graduated from the Faculty of Engineering, Aichi Institute of Technology, Toyota, Japan, in 1989. In 1994, he joined TOYO Electric Corporation, where he is currently a R&D Manager. He is also leading several R&D projects and commercial products related to free-space optics and underwater visible light communications. He is a Member of IEICE.